Atmospheric
Chemistry
and Physics
Discussions

Open Access

EGU

Contribution of the gas-phase reaction between hydroxyl radical and sulfur dioxide to the sulfate aerosol over West Pacific

Yu-Wen Chen[1], Yi-Chun Chen[1], Charles C.-K. Chou[1], Hui-Ming Hung[2], Shih-Yu Chang[3], Lisa Eirenschmalz[4], Michael Lichtenstern[4], Helmut Ziereis[4], Hans Schlager[4], Greta Stratmann[4,#], Katharina Kaiser[5,6], Johannes Schneider[6], Stephan Borrmann[5,6], Florian Obersteiner[7], Eric Förster[7], Andreas Zahn[7], Wei-Nai Chen[1], Po-Hsiung Lin[2], Shuenn-Chin Chang[8], Maria Dolores Andrés Hernández[9], Pao-Kuan Wang[1], and John P. Burrows[9]

[1] Research Center for Environmental Changes, Academia Sinica, Taipei, Taiwan

[2] Department of Atmospheric Sciences, National Taiwan University, Taipei, Taiwan

[3] Department of Public Health, Chung Shan Medical University, Taichung, Taiwan

[4] Institute of Atmospheric Physics, German Aerospace Center, Wessling, Germany

[5] Institute for Atmospheric Physics, Johannes Gutenberg-University, Mainz, Germany

[6] Max Planck Institute for Chemistry, Mainz, Germany

[7] Institute of Meteorology and Climate Research, Karlsruhe Institute of Technology, Karlsruhe, Germany

[8] Environmental Protection Administration, Taipei, Taiwan

[9] Institute of Environmental Physics, University Bremen, Bremen, Germany

[#] Now at German Electron Synchrotron, Hamburg, Germany

Correspondence to: Yi-Chun Chen (yichunchen@gate.sinica.edu.tw) and Charles C.-K. Chou (ckchou@gate.sinica.edu.tw)

Abstract. Sulfate is among the major components of atmospheric aerosols or fine particulate matters. Aerosols loaded with sulfate result in low air quality, damage to ecosystems, and influences on climate change. Sulfate aerosols could originate from that directly emitted to the atmosphere and that produced by atmospheric physicochemical processes. The latter is generated from sulfur dioxide (SO_2) via oxidation either in the gas phase reactions or in the aqueous phase. Several mechanisms of SO_2

25   oxidation have been proposed, but the differentiation of the various mechanisms and identification of the sources remain challenging. To meet this need, a new method to estimate the contribution of the gas-phase reaction between hydroxyl radical (OH) and SO_2 to the sulfate aerosol is proposed and investigated. Briefly, we consider the OH-reaction rates of the respective trace gases that compete for OH radicals with SO_2 in the troposphere, and estimate the fraction of SO_2-OH reaction in the total OH reactivity. Then the relationship between sulfate concentration and the SO_2-OH reaction is analyzed statistically to

30   investigate the sources of sulfate in aerosols. We test this method using the data from ground-based observations and aircraft measurements made during the Effect of Megacities on the transport and transformation of pollutants on the Regional to Global scales in Asia (EMeRGe-Asia) over the western Taiwan and West Pacific regions. Our results show that the estimated SO_2-OH reactivity fraction is well-correlated with sulfate concentration. The sulfate production from SO_2-OH reaction accounts for approximately 30% of the total sulfate in aerosols collected at the surface and near-surface (altitude < 600 m) in our study

35   area, comparable to the estimates from other model simulations. Within its assumptions and limitations, this new method provides a valuable approach to investigate the significance of SO_2-OH reaction regionally and globally.

Atmospheric
Chemistry
and Physics
Discussions

Open Access

EGU

1 Introduction

Sulfate aerosol is a dominant component of particulate matters that significantly influences environmental issues, such as air

quality, climate change, human health, and acid deposition. Sulfate is an important part of acid rain and ecosystem

40 acidification, resulting from sulfur deposition (Greaver et al., 2012; Gorham et al., 1984). Using the average sulfate

concentrations measured from five cities in western Taiwan during 2017 - 2020, reported by the Environmental Protection

Administration of Taiwan, sulfate accounts for approximately 20% by weight of atmospheric particulate matters with a

diameter less than 2.5 micrometers ($PM_{2.5}$).

45 Understanding the origin of sulfate is an essential prerequisite for governments to develop an environmental policy that reduces

air pollution and improves air quality and human health. Sulfate aerosol can be divided into two categories known as primary

sulfate and secondary sulfate. The major sources of primary sulfate include sea sprays, thermal power plants, and volcanic

eruptions (Allen et al., 2002), whereas sulfur dioxide (SO_2) is the dominant precursor of secondary sulfate through gas-phase

oxidation and aqueous-phase oxidation (Stockwell et al., 2012).

50

There are primarily two mechanisms by which SO_2 is oxidized in the atmosphere. These comprise both gas-phase and aqueous-

phase reactions. Though oxygen (O_2) is the most abundant oxidant in the troposphere, the significant energy barrier of the

SO_2-O_2 endothermic reaction slows the reaction rate at atmospheric temperatures, making the reaction of O_2 with SO_2 of minor

importance (Hindiyarti et al., 2007). Similarly, the reaction rate coefficients of oxidation of SO_2 with ozone (O_3) and the

55 hydroperoxyl radical (HO_2) are also of negligible importance. Hydroxyl radical (OH), though having concentrations much

smaller than that of O_2, is the most important gas-phase oxidant for SO_2 oxidation (Stockwell and Calvert, 1983). SO_2 is first

oxidized to $HOSO_2$ by a termolecular reaction involving an inert reaction partner (M) to take up excess kinetic energy. $HOSO_2$

then reacts with O_2 in the air to form sulfur trioxide (SO_3) and release an HO_2. Other oxidants that could also oxidize SO_2 include stabilized Criegee intermediates (Boy et al., 2013; Kurtén et al., 2011; Ye et al., 2018), organic peroxy radicals (RO_2,

60   where R is an unspecified organic group) (Kurtén et al., 2011; Kan et al., 1981), and superoxide ions (O_2^-) (Tsona et al., 2018). SO_3 then reacts with water vapor (H_2O) in the gas phase to form sulfuric acid (H_2SO_4). SO_3 may also react directly with H_2O on the wet surface of aerosols or rain droplets to form H_2SO_4.

In contrast to the gas phase oxidation of SO_2 in the atmosphere, the aqueous-phase oxidation mechanisms of SO_2 are not as well understood. This is in part related to the relatively high solubility of SO_2 and large dissociation equilibrium constants.

65   Specifically, SO_2 is soluble, having a Henry's Law constant of approximately 1.2 to 1.5 mol $kg^{-1} \cdot bar^{-1}$ (Hoffmann and Jacob, 1984; Sander et al., 2006; Dean, 1992). It dissociates to bisulfite ions (HSO_3^-) and sulfite ions (SO_3^{2-}) in an aqueous solution. A variety of plausible pathways to form $SO_2 \cdot H_2O$, HSO_3^-, and SO_3^{2-} have been proposed. For example, dissolved O_3 is reported to oxidize dissolved SO_2 with a rate coefficient depending significantly on the pH of the solution (Maahs, 1983; Hoyle et al., 2016). Moreover, in the presence of some transition metals acting as catalysts, such as iron ions (Fe^{3+}) and

70   manganese ions (Mn^{2+}), dissolved O_2 can oxidize SO_2 efficiently (Herrmann et al., 2000; Harris et al., 2013; Brandt and van Eldik, 1995). Hydrogen peroxide (H_2O_2) (Kunen et al., 1983) and organic peroxides (Wang et al., 2019; Dovrou et al., 2019) are also soluble and important oxidants in aqueous solutions such as tropospheric aerosols and rain droplets. They react with HSO_3^- ions to form SO_4^{2-} ions. The SO_2 related dissociated sulfur-containing ions are oxidized as well by the OH radical through chain reactions (McElroy, 1986). Besides, recent reports suggest that SO_2 oxidation also occurs on interfacial surfaces

75   of acidic micro-droplets in the absence of other oxidants at pH < 3.5 (Hung et al., 2018), and that nitrogen dioxide (NO_2) can oxidize SO_2 in droplets in the presence of NH_3 (Ge et al., 2019).

Atmospheric
Chemistry
and Physics
Discussions

Despite the progress made on our understanding of the mechanisms by which SO_2 is oxidized in the gas-phase and aqueous-phase, the contributions of the respective mechanisms to the total atmospheric sulfate concentrations remain unclear. This

80 research aims to improve the current understanding of SO_2 gas-phase oxidation by enabling the fraction of gas phase and thus also aqueous phase oxidation to be estimated accurately. We develop an approach that addresses the competition for key atmospheric oxidants between SO_2 and other important trace gases. Several assumptions and approximations are made to determine the fraction of OH reacting with SO_2 in the gas phase. This we call the gas-phase reaction rate fraction and is denoted as $f_{SO2\text{-}OH}$ hereafter. With the ground observation in Taiwan and aircraft measurements from EMeRGe-Asia field campaign

85 on-board the HALO research aircraft of DLR (HALO, https://www.dlr.de/content/de/missionen/halo.html), the values of $f_{SO2\text{-}OH}$ at the surface and in the air are calculated, which are further utilized to estimate the contribution of the SO_2-OH reaction to the total production of sulfate. This method is applied to areas within Taiwan and outside of Taiwan to verify its reliability and versatility.

2 Data description

90 ### 2.1 EMeRGe-Asia data

The Effect of Megacities on the transport and transformation of pollutants on the Regional to Global scales over Asia (EMeRGe-Asia) was a field experiment led by the University of Bremen, Germany, conducted in collaboration with Academia Sinica, Taiwan. The EMeRGe-Asia aircraft field campaign took place from Taiwan, from March 10th to April 9th in 2018. This field campaign investigated the composition and influence of pollution plumes from major population centers in Eastern and

95 Southeastern Asia utilizing the HALO aircraft research platform (see flight tracks in Fig. S1). Trace gases, including carbon monoxide (CO), nitrogen monoxide (NO), the sum of reactive nitrogen oxides (NO_y), peroxyacetyl nitrate (PAN), volatile organic compounds (VOCs), SO_2, and O_3, as well as sulfate aerosol (diameter from 40 to 1000 nm) mass concentrations, were

Atmospheric
Chemistry
and Physics
Discussions

analyzed in this study. VOCs measured during the campaign included formaldehyde (CH_2O), methanol (CH_3OH), acetonitrile (CH_3CN), acetaldehyde (CH_3CHO), acetone (CH_3OCH_3), isoprene (C_5H_8), benzene (C_6H_6), toluene (C_7H_8), and xylene (C_8H_{10}). Details of these measurements are listed in Table 1. All the data are reanalyzed to obtain a consistent 1-minute average dataset if there is no specific clarification. In addition, the altitudes of airmasses are rounded to hundred meters for classification.

Although most of the measurements during the campaign were taken over a large area of the West Pacific, from the Philippines to Japan, there were many regular measurements made over Western Taiwan, typically at an altitude of approximately 600 m. This study focuses on this area and these altitudes. Measurements in this area were mainly carried out between 8:00 to 17:00 (in local standard time, LST); sparse measurements performed outside this period are excluded from the 1-minute average dataset.

2.2 Surface observational data

Hourly ambient concentrations of trace gases, including CO, SO_2, NO, NO_2, NO_x, and O_3, measured at the air quality stations of the Taiwan Environmental Protection Administration (EPA), are analyzed in this study. The hourly data observed between 8:00 to 17:00 LST from March 17th to April 7th of 2018 are included in our analyses to compare the surface observations with the airborne measurements. Further information on the instrumentation at the surface stations is listed in Table S1. In addition, samples of fine particulate matters (i.e., $PM_{2.5}$) were collected at 11 sites distributed in central western Taiwan during the campaign period (from March 13th to March 31st, 2018). The chemical composition of the $PM_{2.5}$ samples was analyzed in the laboratories of RCEC, Academia Sinica, and the daytime (8:00 to 19:00 LST) sulfate concentration is used in this study. The field sampling and in-lab chemical analyses are as described in Salvador and Chou (2014). The geographic locations where we sampled $PM_{2.5}$ are illustrated in Fig. S2.

3 Data analysis and assumptions

120 In this study, OH radical is assumed to be the dominant tropospheric oxidant of SO_2 in the gas-phase. It is challenging to

quantify the reaction rate of SO_2-OH oxidation directly as sophisticated instruments are necessary to accurately measure OH

radicals. Though model simulation provides information about OH radical concentration, discrepancies remain between model

results and observations (e.g., Griffith et al., 2016; Lew et al., 2020). OH oxidizes not only SO_2 but also many other trace gases

in the air, such as methane (CH_4), CO, NO, NO_2, and VOCs. We examine the competition for OH radicals among these trace

125 gases to estimate the fraction of OH reacting with SO_2, i.e., $f_{SO2\text{-}OH}$.

We estimate the $f_{SO2\text{-}OH}$ as defined by Eq. (1), where OH reactions with major trace gases (CH_4, CO, NO, NO_2, VOCs, and

SO_2) are considered. This method constrains any overestimation of SO_2 oxidation rate in the absence of accurate knowledge

about the concentration of OH radicals in air masses. The OH-trace gas reactions are either second-order reactions (CH_4, CO,

130 NO, and NO_2) or third-order reactions involving air as the third body. The SO_2-OH reaction is such a third-order reaction but

is considered a pseudo-second-order reaction at low altitudes because of a reasonable approximation that the nitrogen (N_2) and

O_2 have stable concentrations over a small altitude range. As a result, Eqs. (2)-(7) describe the OH reaction rate of each major

trace gas by three parameters, including the rate coefficient, the concentration of the trace gas, and the concentration of OH

radical. The rate constants of these OH reactions are summarized in Table S2 (Burkholder et al., 2020).

135 $$f_{SO2\text{-}OH} = \frac{r_{SO_2-OH}}{r_{CH_4-OH} + r_{CO-OH} + r_{NO-OH} + r_{NO_2-OH} + r_{VOCs-OH} + r_{SO_2-OH}} \qquad (1)$$

$$r_{CH_4-OH} = k_{CH_4}[CH_4][OH] \qquad (2)$$

$$r_{CO-OH} = k_{CO}[CO][OH] \qquad (3)$$

$$r_{NO-OH} = k_{NO}[NO][OH] \qquad (4)$$

$$r_{NO_2-OH} = k_{NO_2}[NO_2][OH] \qquad (5)$$

140 $$r_{VOCs-OH} = \sum k_{VOCs}[VOCs][OH] \tag{6}$$

$$r_{SO_2-OH} = k_{SO_2}[SO_2][OH] \tag{7}$$

Among the major trace gases considered here, VOCs are not measured at the ground-based stations of Taiwan EPA. Although

the concentrations of some VOCs were measured onboard HALO and the sum of the measured concentrations may represent

145 the majority of the VOCs to a reasonable approximation, significant uncertainty could still remain in the estimate of f_{SO2-OH} in

case of missing one or some of the key VOCs. Considering the challenge and difficulty of measuring all the significant VOCs,

we propose a different approach. We assume that the total OH reactivity of VOCs (Eq. (6)) is proportional to the sum of OH

reactivity of other trace gases (Eq. (2)-(5) and (7)), as written in Eq. (8).

$$r_{VOCs-OH} \approx t \left(r_{CH_4-OH} + r_{CO-OH} + r_{NO-OH} + r_{NO_2-OH} + r_{SO_2-OH} \right) \tag{8}$$

150

This assumption is consistent with previous observations in urban areas (Yang et al., 2017). In addition, the analysis using the

measurements of the EMeRGe-Asia campaign also indicates that the total OH reactivity of the measured VOCs is linearly

correlated to that contributed by other major gaseous pollutants, i.e., CO, NO, NO_2, SO_2, and CH_4 (see Fig. S3). Consequently,

the f_{SO2-OH} is redefined as Eq. (9) by applying the above assumptions.

155 $$f_{SO2-OH} = \frac{r_{SO_2-OH}}{(r_{CH_4-OH}+r_{CO-OH}+r_{NO-OH}+r_{NO_2-OH}+r_{SO_2-OH}) \times (1+t)} \tag{9}$$

Because the proportional parameter "t" for OH-VOCs reactions in Eq. (9) is difficult to be determined accurately and because

the observations for VOCs are not available at the ground-based stations, we further simplify Eq. (9) to Eq. (10) by ignoring

that scaling factor. Thus Eq. (10) gives an approximation of f_{SO2-OH}, which is denoted as $f_{SO2-OH}{}^{*}$.

160 $$f_{SO2-OH}{}^{*} = \frac{r_{SO_2-OH}}{r_{CH_4-OH}+r_{CO-OH}+r_{NO-OH}+r_{NO_2-OH}+r_{SO_2-OH}} \tag{10}$$

Eq. (10) is transformed to Eq. (11) by dividing each component in the numerator and denominator by $k_{SO_2}[SO_2][OH]$, suggesting that the average ratios of each trace gas over SO_2 are required to calculate $f_{SO2\text{-}OH}{}^{*}$. These ratios are derived from field measurements in this study with the slope of linear regression using the least-squares method. However, the fits have

165   significant errors for most trace gases, which means that the derived slopes might be arguable. These low correlations may result from different weather conditions, solar radiation intensity, and instrumental detection limits (see Table S1), discussed in Section 4.1. Here, it is assumed that the air parcels achieve a quasi-stationary state and the O_3 concentration represents a measure of the oxidizing capacity of such air masses. This implies that the concentration of each trace gas divided by the concentration of O_3 can be viewed as the relative amount of reductant. Consequently, Eq. (11) yields into Eq. (12). With this

170   transformation, the performance of linear regression improves considerably as discussed in section 4.1.

$$f_{SO2\text{-}OH}{}^{*} = \frac{1}{k'_{CH_4}\frac{[CH_4]}{[SO_2]}+k'_{CO}\frac{[CO]}{[SO_2]}+k'_{NO}\frac{[NO]}{[SO_2]}+k'_{NO_2}\frac{[NO_2]}{[SO_2]}+1} \tag{11}$$

(k' of each trace gas is the ratio of the rate coefficient of the OH reaction with that gas to that for SO_2, i.e., k_{SO2}.)

$$f_{SO2\text{-}OH}{}^{*} = \frac{1}{k'_{CH_4}\frac{[CH_4]/[O_3]}{[SO_2]/[O_3]}+k'_{CO}\frac{[CO]/[O_3]}{[SO_2]/[O_3]}+k'_{NO}\frac{[NO]/[O_3]}{[SO_2]/[O_3]}+k'_{NO_2}\frac{[NO_2]/[O_3]}{[SO_2]/[O_3]}+1} \tag{12}$$

175

As the reaction rate of the reaction CH_4-OH is less than that of reactions CO-OH, NO-OH, and NO_2-OH (see Table S2 for details), the influence of the reaction of CH_4-OH is assumed negligible and is thus ignored in the calculation. Consequently, only three relationships (CO/O_3-SO_2/O_3, NO/O_3-SO_2/O_3, and NO_2/O_3-SO_2/O_3) are required to approximate the $f_{SO2\text{-}OH}{}^{*}$, as shown in Eq. (13). This equation is further utilized in surface and airborne observations in this study.

180   $$f_{SO2\text{-}OH}{}^{*} = \frac{1}{k'_{CO}\frac{[CO]/[O_3]}{[SO_2]/[O_3]}+k'_{NO}\frac{[NO]/[O_3]}{[SO_2]/[O_3]}+k'_{NO_2}\frac{[NO_2]/[O_3]}{[SO_2]/[O_3]}+1} \tag{13}$$

The airborne NO_2 is approximated by subtracting NO and PAN from NO_y, assuming that NO_y is composed of NO, NO_2, and PAN in the daytime, whereas HNO_3 exists mainly in the form of particulate nitrate. However, there are fewer PAN measurements than that of NO and NO_y. Consequently, we determine the PAN-NO_y slope within specified region and altitude

185 to estimate the proportion of PAN in NO_y (shown in Fig. S4). Then the airborne NO_2 is approximated according to Eq. (14):

$$\text{Approximated airborne } NO_2 = NO_y \times (1 - slope_{PAN-NO_y}) - NO \qquad (14)$$

4 Results and discussion

4.1 Importance of normalization by O_3

We assume that the observed air plume was in steady-state, and that the ambient O_3 concentration was representative of the

190 tropospheric oxidizing capacity of the air masses. Fig. 1 demonstrates the CO-SO_2, NO-SO_2, and NO_2-SO_2 relationships before and after the O_3 normalization using data from the Tainan station located in southwestern Taiwan. Low correlations between these trace gases before the O_3 normalization (Fig. 1a, 1c, 1e) are in part explained by the different weather conditions and solar radiation. For example, the photochemical consumption of air pollutants in the air masses from pollution sources traveling to the observation stations can diverge under different weather conditions, leading to different aging of the plume. The inter-

195 species correlation significantly improved after normalization by O_3 (Fig. 1b, 1d, 1f). These differences suggest that the inter-species correlation is likely subject to atmospheric oxidation, and the O_3-normalization approach can efficiently reduce the relevant interferences. Taking the stations located in western Taiwan into account, R^2 of CO-SO_2, NO-SO_2, and NO_2-SO_2 increase from 0.062, 0.061, and 0.109 to 0.468, 0.428, and 0.531, respectively, after normalizing by ozone. The individual values for each station and trace gas are illustrated in Fig. S5.

200

Atmospheric
Chemistry
and Physics
Discussions

The normalization of the airborne measurements leads to the same effects. We divide western Taiwan into five regions, as shown in Fig. S6, where the airborne measurement is distributed. With aircraft-observed data in these regions, the trace gases-SO_2 relationships are determined with the O_3 normalization method. The average R^2 of CO-SO_2, NO-SO_2, and NO_2-SO_2 for the five regions increased from 0.397, 0.698, and 0.614 to 0.672, 0.723, and 0.726, respectively, after the ozone normalization.

205   The higher values of R^2 after the O_3 normalization imply that slopes have an improved accuracy which propagates into the calculation of $f_{SO2\text{-}OH}^*$.

4.2 Relationship between SO_2–OH reaction and sulfate concentration in Western Taiwan

We use the computed slopes from the plots of CO/O_3-SO_2/O_3, NO/O_3-SO_2/O_3, and NO_2/O_3-SO_2/O_3 to estimate the values of $f_{SO2\text{-}OH}^*$ for surface stations by using Eq. (13), which are then compared with the sulfate concentrations. As shown in Fig. 2a,

210   the sulfate concentration positively correlates with $f_{SO2\text{-}OH}^*$ measured at 11 surface stations. This correlation implies that SO_2–OH reaction explains the sulfate variability to a significant extent at selected locations. The regression slopes would be close to zero if the contribution of SO_2–OH reaction to sulfate was negligible. The regression intercept is explained as the amount of sulfate independent of SO_2–OH reaction, e.g., primary sulfate, transported sulfate, and sulfate derived from aqueous SO_2 oxidation.

215

The importance of the difference in weather conditions and the origin of the transported air plumes is now considered. Three periods with similar weather conditions are investigated. The weather type is considered to describe the daily synoptic weather event log, obtained from the Taiwan Atmospheric event Database (Su et al., 2018). The first period under consideration was March 13rd, 14th, and 17th – 19th, during which the southwesterly flow of air was dominant. The second period includes March

220   16th, 22nd, and 27th, which is under northeasterly flow. The third period comprises March 23rd – 26th, 28th, and 29th, which contains weak synoptic weather events. The correlations of $f_{SO2\text{-}OH}^*$ and the amount of sulfate during these three periods are

11

higher than that for the entire observation period, as shown in Fig. 3. This indicates that weather conditions influence the

formation of sulfate.

225   For the airborne observation data, we divided Western Taiwan into five regions (as shown in Fig. S6) and calculated the $f_{SO2\text{-}OH}^*$ separately. A positive correlation between sulfate and $f_{SO2\text{-}OH}^*$ is also observed in the airborne observation, as shown in

Fig. 2b. As the derived positive slope is marginally significant (p-value = 0.218), sulfate and $f_{SO2\text{-}OH}^*$ analyses with adequate

airborne measurement data are necessary to validate the relationship. We therefore extend the study to a larger region over the

West Pacific in Sect. 4.3.

230   **4.3 Relationship between SO_2–OH reaction and sulfate concentration over the West Pacific**

Considering aircraft speed, here a 15-second average dataset (instead of a 1-minute average in the previous analysis) is utilized

to improve the spatial resolution. In addition, the data is classified according to their longitude and latitude; the data located

within a $0.25°$ x $0.25°$ gridded region is used to calculate the $f_{SO2\text{-}OH}^*$. The contribution of SO_2–OH reaction is evaluated at

different altitudes and regions, including Taiwan, East China Sea, and South Japan Sea, as presented in Fig. 4. A significant

235   correlation between sulfate and $f_{SO2\text{-}OH}^*$ is found in various regions and altitudes, and the information is presented in Table 2.

Although a strong correlation exists at different altitudes, no significant trends exist between altitudes and other variables. We

expect the $f_{SO2\text{-}OH}^*$ to decrease with height as trace gases' concentrations are generally higher near to the surface. However,

the calculated maximum $f_{SO2\text{-}OH}^*$ does not decrease with altitude. This discrepancy may result from using measurements from

240   different locations and the existence of inversion layers, which influences the distribution of trace gases. It is noteworthy that,

a special multi-altitudes (600 m, 900m, 1200 m) flight mission conducted over western Taiwan on April 3rd revealed the largest

value of slope of sulfate vs. $f_{SO2\text{-}OH}{}^*$ at 900 m (shown in Fig. 4f). This phenomenon may be explained by the accumulation of trace gases below the ceiling of the boundary layer near 900 m.

4.4 OH-oxidation explicable sulfate percentage

245   According to our hypothesis, the intercept of the plot of sulfate vs. $f_{SO2\text{-}OH}{}^*$ may approximate the amount of sulfate generated by mechanisms other than the SO_2–OH reaction. This includes SO_2 aqueous-phase oxidation, primary source emission, and transport. For environmental policy issues, it is valuable and necessary to separate the contribution of SO_2 gas-phase oxidation from the other sulfate sources. As a result, the SO_2 gas-phase-produced sulfate (SGS) percentage is defined in Eq. (15), enabling us to investigate the extent of SO_2 gas-phase oxidation in different areas.

250   SO_2 gas-phase-produced sulfate (SGS) percentage $= \dfrac{\text{maximum sulfate in target area - intercept}}{\text{maximum sulfate in target area}} \times 100\%$ (15)

Table 2 presents the SGS percentage in selected periods at the surface and selected altitudes/areas. The results show that SGS percentages are approximately 30% at the surface and at 600 m over a period of time. This result is comparable with the model simulation by Harris et al. (2013) that 76±7% of SO_2 undergoes aqueous-phase oxidation, and the rest of SO_2 is oxidized by OH radicals in the gas phase. However, for a daily analysis over a specific region, the SGS percentages for data at different

255   altitudes vary and may be much higher than 30% (see Table 2). These high SGS cases could be related to the less amount of transported sulfate. For example, the SGS of Fig. 4d is much higher than that of Fig. 4b, although they were both measured at 300 m. The backward trajectories using HYSPLIT provided by NOAA ARL (Stein et al., 2015; Rolph et al., 2017) in Fig S7a-b show that the air masses of Fig. 4a-b passed through East China and loaded with abundant SO_2 and primary sulfate, while air parcels of the case of Fig. 4c-d went across the Sea of Japan, a relatively clean area. Less transported sulfate in the air

260   parcels could contribute to higher SGS. The high SGS at 700 and 900 m over Taiwan may also connect with low long-range-transported sulfate (see Fig. S7c-d), and thus the importance of the SO_2-OH gas-phase oxidation increase in these cases. Therefore, the amount of primary sulfate could fluctuate and impact the percentage of SO_2 gas-phase-produced sulfate.

Table 2 presents the amount of SGS and the average SO_2 concentration in target areas to enable us to verify our inference of

265   the SGS percentage. With the reported average daytime OH radical concentration of 8.3×10^6 molecules cm^{-3} sampling in

region B from September 2004 to April 2005 (Lin et al., 2010) and the SO_2-OH reaction rate coefficient of 1.7×10^{-12} cm^3

$molecule^{-1} s^{-1}$, the necessary reaction time is calculated to be approximately 3.4 hours at the surface (3/13-3/31) and 2.3 hours

at an altitude of 600 m. The near-surface reaction time for producing the amount of sulfate is adequate for short-range transport

within Taiwan, which justifies our result that nearly 30% of sulfate aerosol mass results from the SO_2-OH reaction.

270   **4.5 Characteristics of trace gases and SO_2 oxidation at the surface and as a function of altitude**

The characteristics of trace gases provide additional information to investigate the possible sources of pollution plumes. For

example, CO-NO_x at the surface and CO-NO_y in the air have similar correlations. As shown in Fig. 5a, the correlations between

CO and NO_x at the surface, as well as CO and NO_y in the air, are similar. The slopes of CO-NO_x at the surface and CO-NO_y

in the air are 0.057 ± 0.0003 and 0.050 ± 0.002, respectively. Though NO_x does not wholly represent NO_y, we infer that NO_x

275   takes a significant part of NO_y. On the other hand, as demonstrated in Fig. 5b-c, discernible disparities exist in SO_2-CO and

SO_2-NO_x/SO_2-NO_y airborne to surface relationships. According to the scatter plots, the SO_2-CO relationship can be generally

subdivided into two categories: high SO_2 to CO ratio and low SO_2 to CO ratio, and so does the SO_2-NO_x/SO_2-NO_y relationship.

These two apparent features are explained by different emission types: traffic sources and industrial sources. Conforming to

the Taiwan Emission Data System version 10.1 (TEDS 10.1, 2020, as listed in Table S3), the annual SO_2 to CO emission ratio

280   of traffic sources (line sources in the TEDS) is estimated to be $4.1x10^{-4}$, and that of industrial sources lie between 0.3 to 20,

which is much higher than the ratio of traffic sources. Similar to the annual SO_2 to CO emission ratio, the annual SO_2 to NO_x

emission ratios of traffic sources and industrial sources are assessed to be $7.7x10^{-4}$ and 0.37 to 0.79, respectively.

According to Fig. 5b-c, airborne trace gases have high SO_2 to CO ratios and high SO_2 to NO_y ratios. These relationships imply

285   that industrial sources may significantly contribute more to the airborne trace gases over Taiwan than traffic sources during

the spring and the intermonsoon weather. The industrial-produced plumes are transported to the upper air more quickly through

the tall stacks of these sources and the thermal driving force than traffic emissions released close to the surface. Here, we

classify the EPA surface stations into five regions defined in Section 4.1 and calculate the average f_{SO2-OH}^* for each region. As

shown in Fig. 6, the orders of f_{SO2-OH}^* at the surface and in the air are B=C>E>D>A and E>B>D>C>A, respectively. Region

290   B has high rate fractions at the surface and in the air since a massive coal-fired power plant and vast industrial areas stand in

region B. The distribution of f_{SO2-OH}^* coincides with the locations of massive power plants and industrial areas, indicating that

industrial sources significantly influence f_{SO2-OH}^* and the sulfate concentrations. Nonetheless, region E has the highest f_{SO2-OH}^*

in the air but is the third highest at the surface. In addition to a coal-fired power plant and industrial areas located in region

E, the other reason for the observed behavior could be the strong prevailing north wind, which transports SO_2 from upwind

295   sources to southern areas and leads to higher sulfate concentration in region E (see Fig. S8 for average wind speeds in each

region). Nevertheless, limited measurements from surface stations and in the air might not represent the whole region. More

observations are necessary to verify our arguments.

5 Conclusions

Our study investigates and presents an approach to evaluate the contribution of SO_2-OH gas-phase reaction to the total sulfate.

300   We use knowledge of the reactions between OH and the major trace gases (SO_2, CO, NO, NO_2) to estimate the fraction of OH

reactivity due to SO_2-OH reaction, f_{SO2-OH}^*. The surface observations over western Taiwan and airborne EMeRGe-Asia field

measurements over the West Pacific are analyzed. This study shows that the value of f_{SO2-OH}^* has a significant correlation with

the sulfate concentration at the surface and 600 m altitude above Taiwan. This correlation also appears in different areas and

altitudes, though more observational data are needed to confirm the significance. Based on the relationship between sulfate

and $f_{SO2\text{-}OH}^*$, it is concluded that approximately 30% of sulfate at the surface and an altitude of 600 m is produced by SO_2-OH

reaction, which could vary significantly with the influences of primary emission or long-range transported sulfate. Meanwhile,

the observations indicate that SO_2 and sulfate from SO_2-OH reaction in the airspace of western Taiwan primarily come from

industrial sources, such as thermal power plants and industrial areas, conforming with the distribution of $f_{SO2\text{-}OH}^*$. Our results

underline the importance of SO_2-OH gas-phase oxidation in sulfate formation, and demonstrate that the method proposed can

potentially be applied to other regions and under different meteorological conditions taking the assumptions and limitations

into account.

6 Data availability

EMeRGe-Asia data are archived in a public password-protected data archive (https://halo-db.pa.op.dlr.de). Taiwan EPA

station data can be found in the environmental open data platform of EPA, Taiwan (https://data.epa.gov.tw). TEDS 10.1 data

are available on the Taiwan Emission Data System website managed by Taiwan EPA (https://teds.epa.gov.tw/TEDS.aspx).

Author contributions

YWC analyzed the data. YWC, YCC, and CKC prepared for the manuscript. YCC and CKC supervised the work. HMH

advised on the study. JPB conceived the EMeRGe project and led the field campaign. The other authors provided measurement

data. All the authors read and improved the manuscript.

Competing interests

The authors declare that they have no conflict of interest.

Atmospheric
Chemistry
and Physics
Discussions

Acknowledgments

References

Allen, A. G., Oppenheimer, C., Ferm, M., Baxter, P. J., Horrocks, L. A., Galle, B., McGonigle, A. J. S., and Duffell, H. J.,
345 Primary sulfate aerosol and associated emissions from Masaya Volcano, Nicaragua, J. Geophys. Res., 107, 4682,
doi:10.1029/2002JD002120, 2002.

Boy, M., Mogensen, D., Smolander, S., Zhou, L., Nieminen, T., Paasonen, P., Plass-Dülmer, C., Sipilä, M., Petäjä, T., Mauldin,
L., Berresheim, H., and Kulmala, M.: Oxidation of SO2 by stabilized Criegee intermediate (sCI) radicals as a crucial source
for atmospheric sulfuric acid concentrations, Atmos. Chem. Phys., 13, 3865-3879, https://doi.org/10.5194/acp-13-3865-2013,
350 2013.

Brandt, C., and van Eldik, R.: Transition Metal-Catalyzed Oxidation of Sulfur(IV) Oxides. Atmospheric-Relevant Processes
and Mechanisms, Chem. Rev., 95, 119-190, https://doi.org/10.1021/cr00033a006, 1995.

Brito, J. and Zahn, A.: An unheated permeation device for calibrating atmospheric VOC measurements, Atmos. Meas. Tech.,
4, 2143–2152, https://doi.org/10.5194/amt-4-2143-2011, 2011.

355 Burkholder, J. B., Sander, S. P., Abbatt, J. P. D., Barker, J. R., Cappa, C., Crounse, J. D., Dibble, T. S.; Huie, R. E.; Kolb, C.
E.; Kurylo, M. J.; Orkin, V. L.; Percival, C. J.; Wilmouth, D. M.; Wine, P. H.: Chemical kinetics and photochemical data for
use in atmospheric studies; evaluation number 19, Pasadena, CA: Jet Propulsion Laboratory, National Aeronautics and Space
Administration, 2020.

Dean, J. A.: Lange's handbook of chemistry, McGraw-Hill New York, 1992.

360 Dovrou, E., Rivera-Rios, J. C., Bates, K. H., and Keutsch, F. N.: Sulfate Formation via Cloud Processing from Isoprene
Hydroxyl Hydroperoxides (ISOPOOH), Env. Sci. & Technol., 53, 12476-12484, https://doi.org/10.1021/acs.est.9b04645,
2019.

Ge, S., Wang, G., Zhang, S., Li, D., Xie, Y., Wu, C., Yuan, Q., Chen, J., and Zhang, H.: Abundant NH3 in China Enhances
Atmospheric HONO Production by Promoting the Heterogeneous Reaction of SO2 with NO2, Env. Sci. & Technol., 53,
365 14339-14347, https://doi.org/10.1021/acs.est.9b04196, 2019.

Gorham, E., Martin, F. B., and Litzau, J. T.: Acid Rain: Ionic Correlations in the Eastern United States, 1980-1981, Science,
225, 407, https://doi.org/10.1126/science.225.4660.407, 1984.

Greaver, T. L., Sullivan, T. J., Herrick, J. D., Barber, M. C., Baron, J. S., Cosby, B. J., Deerhake, M. E., Dennis, R. L., Dubois,
J.-J. B., Goodale, C. L., Herlihy, A. T., Lawrence, G. B., Liu, L., Lynch, J. A., and Novak, K. J.: Ecological effects of nitrogen

370 and sulfur air pollution in the US: what do we know?, Front. Ecol. Envrion., 10, 365-372, https://doi.org/10.1890/110049, 2012.

Harris, E., Sinha, B., van Pinxteren, D., Tilgner, A., Fomba, K. W., Schneider, J., Roth, A., Gnauk, T., Fahlbusch, B., Mertes, S., Lee, T., Collett, J., Foley, S., Borrmann, S., Hoppe, P., and Herrmann, H.: Enhanced Role of Transition Metal Ion Catalysis During In-Cloud Oxidation of SO2, Science, 340, 727, https://doi.org/10.1126/science.1230911, 2013.

375 Herrmann, H., Ervens, B., Jacobi, H. W., Wolke, R., Nowacki, P., and Zellner, R.: CAPRAM2.3: A Chemical Aqueous Phase Radical Mechanism for Tropospheric Chemistry, J. Atoms. Chem., 36, 231-284, https://doi.org/10.1023/A:1006318622743, 2000.

Hindiyarti, L., Glarborg, P., and Marshall, P.: Reactions of SO3 with the O/H Radical Pool under Combustion Conditions, J. Phys. Chem. A, 111, 3984-3991, https://doi.org/10.1021/jp067499p, 2007.

380 Hoffmann, M. R., and Jacob, D. J.: Kinetics and mechanisms of the catalytic oxidation of dissolved sulfur dioxide in aqueous solution: An application to nighttime fog water chemistry, 1984.

Hoyle, C. R., Fuchs, C., Järvinen, E., Saathoff, H., Dias, A., El Haddad, I., Gysel, M., Coburn, S. C., Tröstl, J., Bernhammer, A. K., Bianchi, F., Breitenlechner, M., Corbin, J. C., Craven, J., Donahue, N. M., Duplissy, J., Ehrhart, S., Frege, C., Gordon, H., Höppel, N., Heinritzi, M., Kristensen, T. B., Molteni, U., Nichman, L., Pinterich, T., Prévôt, A. S. H., Simon, M., Slowik, 385 J. G., Steiner, G., Tomé, A., Vogel, A. L., Volkamer, R., Wagner, A. C., Wagner, R., Wexler, A. S., Williamson, C., Winkler, P. M., Yan, C., Amorim, A., Dommen, J., Curtius, J., Gallagher, M. W., Flagan, R. C., Hansel, A., Kirkby, J., Kulmala, M., Möhler, O., Stratmann, F., Worsnop, D. R., and Baltensperger, U.: Aqueous phase oxidation of sulphur dioxide by ozone in cloud droplets, Atmos. Chem. Phys., 16, 1693-1712, https://doi.org/10.5194/acp-16-1693-2016, 2016.

Hung, H.-M., Hsu, M.-N., and Hoffmann, M. R.: Quantification of SO2 Oxidation on Interfacial Surfaces of Acidic Micro-390 Droplets: Implication for Ambient Sulfate Formation, Env. Sci. & Technol., 52, 9079-9086, https://doi.org/10.1021/acs.est.8b01391, 2018.

Kan, C. S., Calvert, J. G., and Shaw, J. H.: Oxidation of sulfur dioxide by methylperoxy radicals, J. Phys. Chem., 85, https://doi.org/1126-1132, 10.1021/j150609a011, 1981.

Kunen, S. M., Lazrus, A. L., Kok, G. L., and Heikes, B. G.: Aqueous oxidation of SO2 by hydrogen peroxide, J. Geophys. 395 Res. Oceans, 88, 3671-3674, https://doi.org/10.1029/JC088iC06p03671, 1983.

Kurtén, T., Lane, J. R., Jørgensen, S., and Kjaergaard, H. G.: A Computational Study of the Oxidation of SO2 to SO3 by Gas-Phase Organic Oxidants, J. Phys. Chem. A, 115, 8669-8681, https://doi.org/10.1021/jp203907d, 2011.

Lew, M. M., Rickly, P. S., Bottorff, B. P., Reidy, E., Sklaveniti, S., Léonardis, T., Locoge N., Dusanter S., Kundu S., Wood E., and Stevens, P. S.: OH and HO2 radical chemistry in a midlatitude forest: measurements and model comparisons, Atmos.
400 Chem. Phys., 20, 9209–9230, https://doi.org/10.5194/acp-20-9209-2020, 2020.

Lin, Y. C., Cheng, M. T., Lin, W. H., Lan, Y.-Y., and Tsuang, B.-J.: Causes of the elevated nitrate aerosol levels during episodic days in Taichung urban area, Taiwan, Atoms. Environ., 44, 1632-1640, https://doi.org/10.1016/j.atmosenv.2010.01.039, 2010.

Luke, W. T., Kelley, P., Lefer, B. L., Flynn, J., Rappenglück, B., Leuchner, M., Dibb, J. E., Ziemba, L. D., Anderson, C. H.,
405 and Buhr, M.: Measurements of primary trace gases and NOY composition in Houston, Texas, Atoms. Environ., 44, 4068-4080, https://doi.org/10.1016/j.atmosenv.2009.08.014, 2010.

Maahs, H. G.: Kinetics and mechanism of the oxidation of S(IV) by ozone in aqueous solution with particular reference to SO2 conversion in nonurban tropospheric clouds, J. Geophys. Res. Oceans, 88, 10721-10732, https://doi.org/10.1029/JC088iC15p10721, 1983.

410 McElroy, W. J.: The aqueous oxidation of SO2 by OH radicals, Atoms. Environ. (1967), 20, 323-330, https://doi.org/10.1016/0004-6981(86)90034-X, 1986.

Rolph, G., Stein, A., and Stunder, B.: Real-time Environmental Applications and Display sYstem: READY. Environmental Modelling & Software, 95, 210-228, https://doi.org/10.1016/j.envsoft.2017.06.025, 2017.

Salvador, C. M., and Chou, C. C. K.: Analysis of semi-volatile materials (SVM) in fine particulate matter, Atoms. Environ.,
415 95, 288-295, https://doi.org/10.1016/j.atmosenv.2014.06.046, 2014.

Sander, S., Golden, D., Kurylo, M., Moortgat, G., Wine, P., Ravishankara, A., Kolb, C., Molina, M., Finlayson-Pitts, B., and Huie, R.: Chemical kinetics and photochemical data for use in atmospheric studies evaluation number 15, Pasadena, CA: Jet Propulsion Laboratory, National Aeronautics and Space, 2006.

Sander, S. P., and Seinfeld, J. H.: Chemical kinetics of homogeneous atmospheric oxidation of sulfur dioxide, Env. Sci. &
420 Technol., 10, 1114-1123, 1976.

Schulz, C., Schneider, J., Amorim Holanda, B., Appel, O., Costa, A., Sá, S. S. D., Dreiling, V., Fütterer D., Jurkat-Witschas, T., Klimach, T., Knote, C., Krämer M., Martin, S. T., Mertes, S., Pöhlker M. L., Sauer, D., Voigt, C., Walser, A., Weinzierl, B., Ziereis, H., Zöger M., Andreae, M. O., Artaxo, P., Machado, L. A. T., Pöschl U., Wendisch, M., and Borrmann, S.: Aircraft-based observations of isoprene-epoxydiol-derived secondary organic aerosol (IEPOX-SOA) in the tropical upper troposphere
425 over the Amazon region, Atmos. Chem. Phys., 18, 14979-15001, https://doi.org/10.5194/acp-18-14979-2018, 2018.

Speidel, M., Nau, R., Arnold, F., Schlager, H., and Stohl, A.: Sulfur dioxide measurements in the lower, middle and upper troposphere: Deployment of an aircraft-based chemical ionization mass spectrometer with permanent in-flight calibration, Atoms. Environ., 41, 2427-2437, https://doi.org/10.1016/j.atmosenv.2006.07.047, 2007.

430   Stein, A.F., Draxler, R.R, Rolph, G.D., Stunder, B.J.B., Cohen, M.D., and Ngan, F.: NOAA's HYSPLIT atmospheric transport and dispersion modeling system, Bull. Amer. Meteor. Soc., 96, 2059-2077, http://sci-hub.tw/10.1175/BAMS-D-14-00110.1, 2015.

Stockwell, W. R. and Calvert, J. G.: The mechanism of the HO-SO2 reaction, Atoms. Environ. (1967), 17, 2231-2235, https://doi.org/10.1016/0004-6981(83)90220-2, 1983.

Stockwell, W. R., Lawson, C. V., Saunders, E., and Goliff, W. S.: A Review of Tropospheric Atmospheric Chemistry and
435   Gas-Phase Chemical Mechanisms for Air Quality Modeling, Atmosphere, 3, https://doi.org/10.3390/atmos3010001, 2012.

Su, S-H, Chu, J-L, Yo, T-S, Lin, L-Y.: Identification of synoptic weather types over Taiwan area with multiple classifiers, Atmos. Sci. Lett., 19, e861, https://doi.org/10.1002/asl.861, 2018.

Tsona, N. T., Li, J., and Du, L.: From O2–Initiated SO2 Oxidation to Sulfate Formation in the Gas Phase, J. Phys. Chem. A, 122, 5781-5788, https://doi.org/10.1021/acs.jpca.8b03381, 2018.

440   Wang, S., Zhou, S., Tao, Y., Tsui, W. G., Ye, J., Yu, J. Z., Murphy, J. G., McNeill, V. F., Abbatt, J. P. D., and Chan, A. W. H.: Organic Peroxides and Sulfur Dioxide in Aerosol: Source of Particulate Sulfate, Env. Sci. & Technol., 53, 10695-10704, https://doi.org/10.1021/acs.est.9b02591, 2019.

Wendisch, M., Pöschl, U., Andreae, M. O., Machado, L. A. T., Albrecht, R., Schlager, H., Rosenfeld, D., Martin, S. T., Abdelmonem, A., Afchine, A., Araùjo, A. C., Artaxo, P., Aufmhoff, H., Barbosa, H. M. J., Borrmann, S., Braga, R., Buchholz,
445   B., Cecchini, M. A., Costa, A., Curtius, J., Dollner, M., Dorf, M., Dreiling, V., Ebert, V., Ehrlich, A., Ewald, F., Fisch, G., Fix, A., Frank, F., Fütterer, D., Heckl, C., Heidelberg, F., Hüneke, T., Jäkel, E., Järvinen, E., Jurkat, T., Kanter, S., Kästner, U., Kenntner, M., Kesselmeier, J., Klimach, T., Knecht, M., Kohl, R., Kölling, T., Krämer, M., Krüger, M., Krisna, T. C., Lavric, J. V., Longo, K., Mahnke, C., Manzi, A. O., Mayer, B., Mertes, S., Minikin, A., Molleker, S., Münch, S., Nillius, B., Pfeilsticker, K., Pöhlker, C., Roiger, A., Rose, D., Rosenow, D., Sauer, D., Schnaiter, M., Schneider, J., Schulz, C., de Souza,
450   R. A. F., Spanu, A., Stock, P., Vila, D., Voigt, C., Walser, A., Walter, D., Weigel, R., Weinzierl, B., Werner, F., Yamasoe, M. A., Ziereis, H., Zinner, T., and Zöger, M.: ACRIDICON–CHUVA Campaign: Studying Tropical Deep Convective Clouds and Precipitation over Amazonia Using the New German Research Aircraft HALO, B. Am. Meteorol. Soc., 97, 1885-1908, https://doi.org/10.1175/BAMS-D-14-00255.1, 2016.

Yang, Y., Shao, M., Keßel, S., Li, Y., Lu, K., Lu, S., Williams, J., Zhang, Y., Zeng, L., Nölscher, A. C., Wu, Y., Wang, X.,

455   and Zheng, J.: How the OH reactivity affects the ozone production efficiency: case studies in Beijing and Heshan, China, Atmos. Chem. Phys., 17, 7127–7142, https://doi.org/10.5194/acp-17-7127-2017, 2017.

Ye, J., Abbatt, J. P. D., and Chan, A. W. H.: Novel pathway of SO2 oxidation in the atmosphere: reactions with monoterpene ozonolysis intermediates and secondary organic aerosol, Atmos. Chem. Phys., 18, 5549-5565, https://doi.org/10.5194/acp-18-5549-2018, 2018.

460   Zahn, A., Weppner, J., Widmann, H., Schlote-Holubek, K., Burger, B., Kühner, T., and Franke, H.: A fast and precise chemiluminescence ozone detector for eddy flux and airborne application, Atmos. Meas. Tech., 5, 363-375, https://doi.org/10.5194/amt-5-363-2012, 2012.

Atmospheric
Chemistry
and Physics
Discussions

Table 1: Information of measurements used from the EMeRGe-Asia field campaign. Institute of Atmospheric Physics Deutsches Zentrum fuer Luft- und Raumfahrt is abbreviated as DLR-IPA; Institute for Meteorology and Climate Research, Karlsruhe Institute of Technology is abbreviated as KIT-IMK; Johannes Gutenberg University Mainz is abbreviated as JGUM; Max Planck Institute for Chemistry is abbreviated as MPIC.

Gas/Parameter	Instrument	Measurement range	Limit of Detection	Time resolution (Hz)	Institution	References
SO$_2$	CI-ITMS		22 ppt	1	DLR-IPA	Speidel et al., 2007
CO, O$_3$	AMTEX		2 ppb (precision) Accuracy: 5%	1	DLR-IPA	Wendisch et al., 2016
NO, NO$_y$	AENEAS	5 pmol/mol –50 nmol/mol	NO accuracy: ~8% at 50 nmol/mol NO$_y$ accuracy: ~7% at 450 nmol/mol	1	DLR-IPA	Wendisch et al., 2016
O$_3$	FAIRO-CI		Precision: 0.3–1.0 % at f = 10 Hz	10	KIT-IMK	Zahn et al., 2012
PAN	GC-ECD		Overall uncertainty > 0.2 ppb +/- 26 %, < 0.2 ppb +/- 59 %	0.0083	DLR-IPA	
VOCs	HKMS		formaldehyde: 213pptv, methanol: 585 pptv, acetonitrile: 18 pptv, acetaldehyde: 53 pptv, acetone: 27 pptv, isoprene: 33 pptv, benzene: 18 pptv, toluene: 19 pptv, xylene: 25 pptv	0.015	KIT-IMK	Brito and Zahn, 2013
Sulfate	C-ToF-AMS	Diameter: 40 – 1000 nm	0.03 µg m^{-3}, STP, A & P : ≈ 30%	0.067	JGUM; MPIC, Particle Chemistry Department	Wendisch et al., 2016; Schulz et al., 2018

* Intercomaprison found limited differences between the two O$_3$ measurements in terms of 1-min average. Considering the up/down time slots of respective instruments during the campaign flights, we use the mean of FAIRO and AMTEX measurements in this study when both are available, which accounts for the majority of our cases. However, in some cases only one of them is available. We use the available data to represent the result and ignore the potential difference.

Atmospheric
Chemistry
and Physics
Discussions
Open Access
EGU

Table 2: SO₂ gas-phase-produced sulfate (SGS) percentage at different altitudes and areas.

	Surface (Central Taiwan)			
Period	03/13-31	03/13-14, 17-19	03/16, 22, 27	03/23-26, 28, 29
Area	Taiwan	Taiwan	Taiwan	Taiwan
SGS ($\mu g/m^3$)	2.1	2.3	3.1	2.9
SGS (%)	22.9±4.5	26.5±4.0	33.2±3.4	27.5±4.5
RH (%)	60.3±0.3	62.4±0.5	62.5±0.7	53.3±0.6
NO (ppb)	2.42±0.07	2.73±0.16	2.42±0.15	1.97±0.09
NO_x (ppb)	14.84±0.20	16.32±0.46	13.91±0.38	13.25±0.29
SO_2 (ppb)	3.07±0.04	3.28±0.08	2.75±0.09	3.04±0.07
Estimated reaction time [1] (hour)	3.4	3.5	5.6	4.7
Max rate fraction	0.013	0.015	0.016	0.022

	Airborne						
Altitude (m)	300	300	500	600	700	900	1200
Period	03/24	03/17	03/30	03/17-04/03	03/30	04/03	04/03
Area	East China Sea	East China Sea	Southern Japan	Taiwan	Taiwan	Taiwan	Taiwan
SGS ($\mu g/m^3$)	1.18	1.55	0.35	0.53	0.84	1.50	0.45
SGS (%)	25.5±1.4	64.2±11.0	54.1±9.9	27.2±13.0	64.5±7.3	71.9±10.4	24.7±4.2
RH (%)	72.8±1.3	82.2±0.9	53.3±1.6	66.1±1.0	54.6±0.5	72.1±1.3	77.1±1.6
NO (ppb)	0.17±0.04	0.09±0.02	0.06±0.00	0.46±0.05	0.68±0.15	1.60±0.46	0.25±0.09
NO_y (ppb)	5.86±0.13	1.37±0.07	1.55±0.03	4.35±0.19	6.21±1.00	5.11±1.14	2.06±0.26
SO_2 (ppb)	1.38±0.06	0.88±0.06	0.29±0.01	1.18±0.11	4.39±1.54	1.71±0.45	0.31±0.09
Estimated reaction time [1] (hour)	4.3	8.9	6.1	2.3	1.0	4.4	7.2
Max rate fraction	0.45	0.12	0.10	0.023	0.090	0.020	0.051

[1] Estimated reaction time is calculated using OH radical concentration of 8.3×10^6 molecules cm^{-3} molecules cm^{-3} and SO₂-OH reaction rate coefficient of 1.7×10^{-12} cm^3 molecule^{-1} s^{-1}.

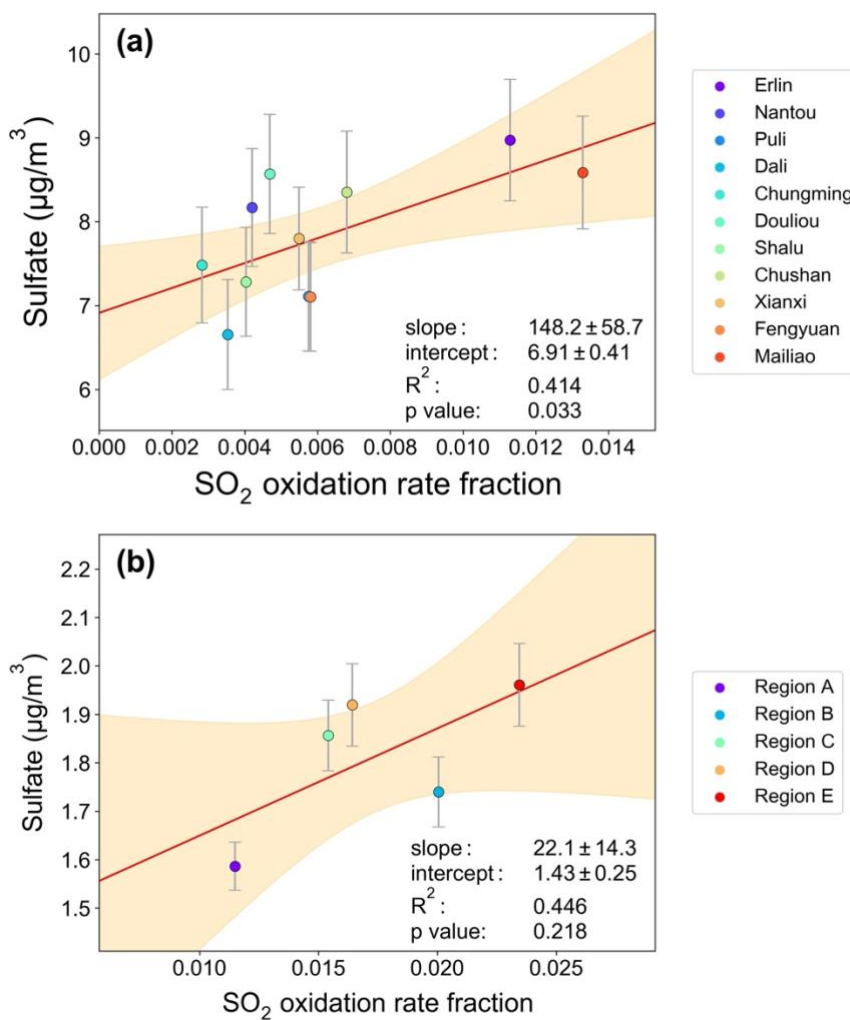475
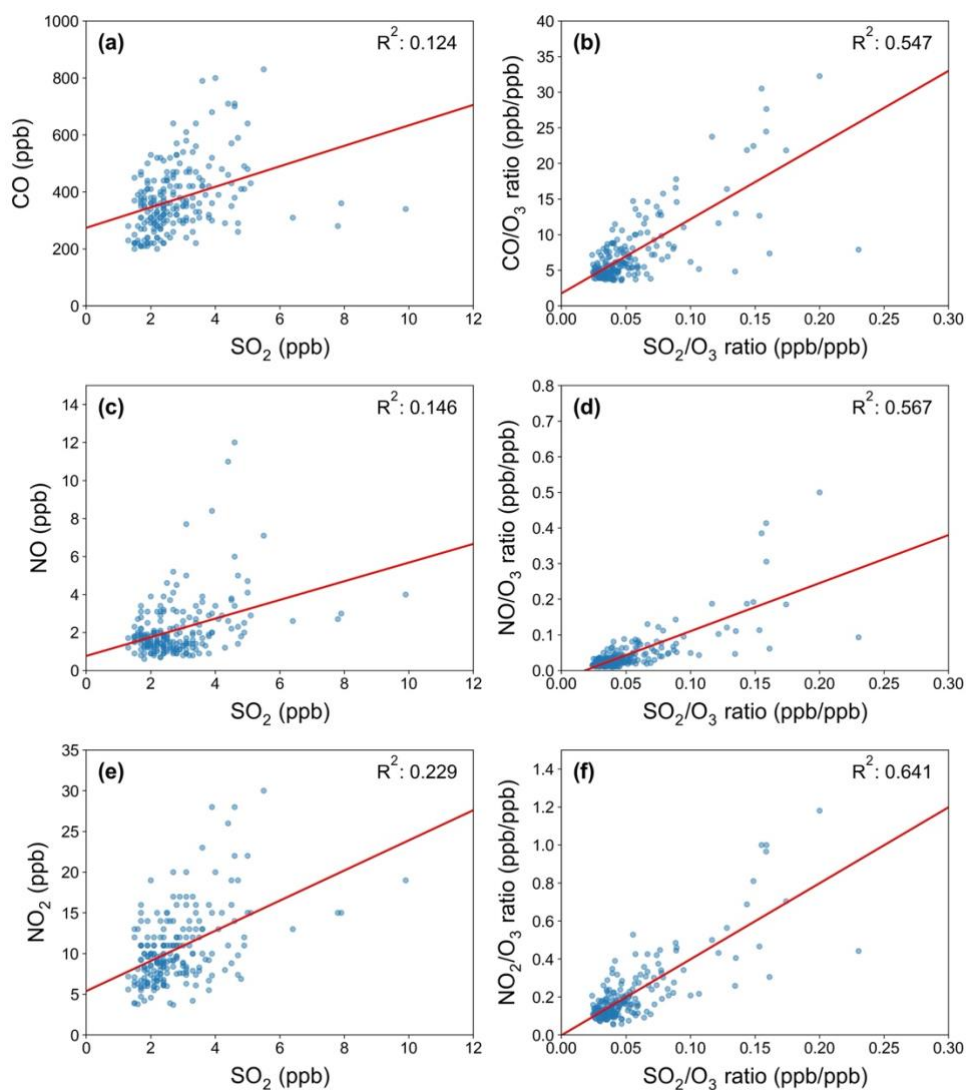
Figure 1: CO-SO₂ (a, b), NO-SO₂ (c, d), and NO₂-SO₂ (e, f) relationships before (a, c, e) and after (b, d, f) the O₃ normalization of Tainan station.

480

Figure 2: Relationships between sulfate concentrations and SO₂ oxidation fraction of rate of loss of OH of (a) surface EPA stations during March 13th to 31st, 2018 and (b) airborne observation from March 17th to April 7th, 2018 (b). Fitting lines are plotted in solid red lines with orange shades of 95% confidential interval.
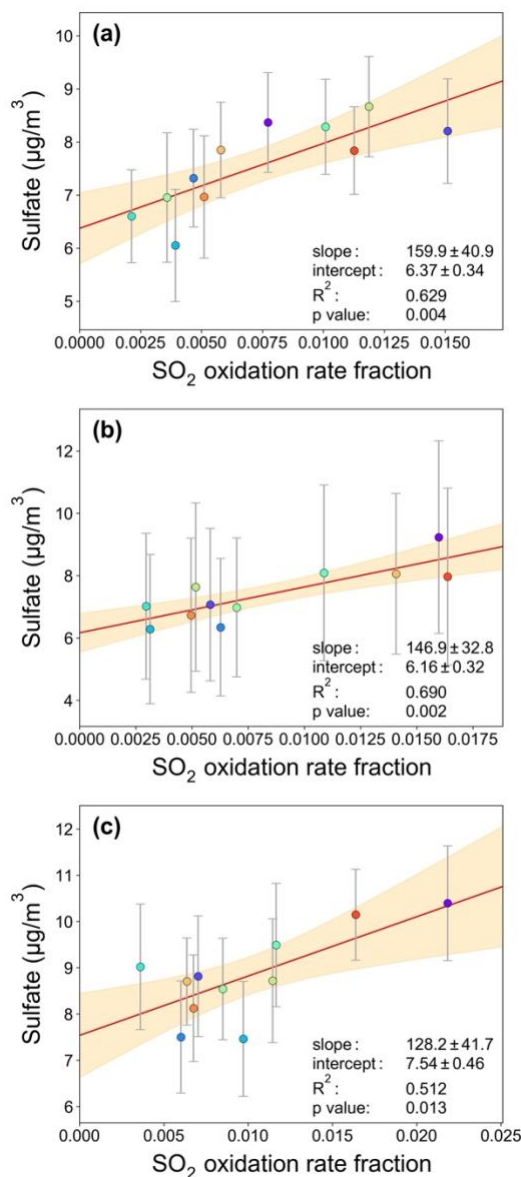
485

Figure 3: Relationships between sulfate concentration and SO₂ oxidation fraction of the rate of OH loss using equation 9 based on surface measurements. The first period (a) consists of March 13rd, 14th, and 17th – 19th, representing the southwesterly flow. The second period (b) includes March 16th, 22nd, and 27th, which serves as the northeasterly flow. The third period (c) corresponds to March 23rd – 26th, 28th, and 29th, representing weak synoptic weather events.

490
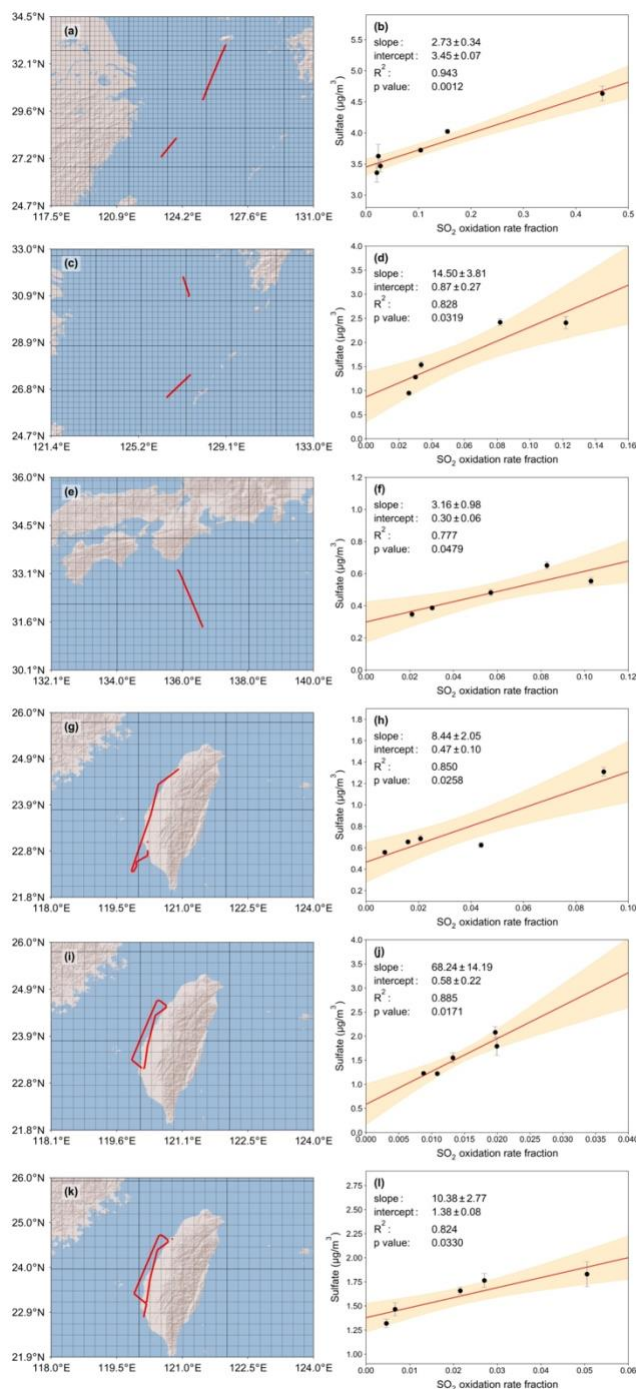
Figure 4: Flight path of data (left) utilized to calculate the correlation of sulfate and SO₂ oxidation fraction of the rate of loss of OH (right). The altitudes of the flights are (a, b) 300 m, (c, d) 300 m, (e, f) 500 m, (g, h) 700 m, (i, j) 900 m, and (k, l) 1200 m, respectively. Noted that a 15-second average dataset (instead of a 1-minute average in the previous analysis) is utilized here. The maps were generated using the Matplotlib Basemap Toolkit version 1.2.0 (https://matplotlib.org/basemap/index.html).

495
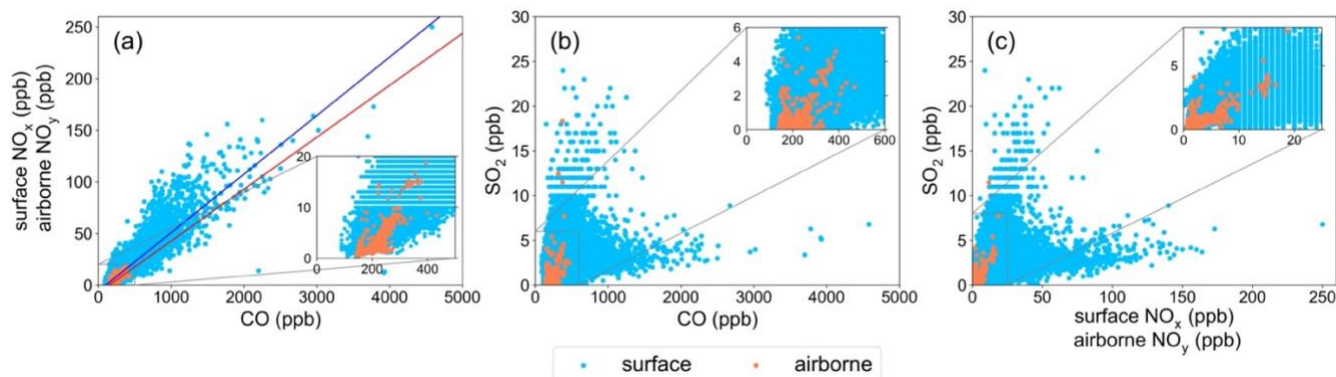
Figure 5: Relationship of ground-based (in blue) and airborne (in red) measurements of (a) NO_x to CO and NO_y to CO, respectively, (b) SO_2 to CO, and (c) SO_2 to NO_x and SO_2 to NO_y, respectively. The slopes of regression lines of surface NO_x to CO and airborne NO_y to CO in 3a are 0.057±0.0003 and 0.050±0.002, respectively.

500
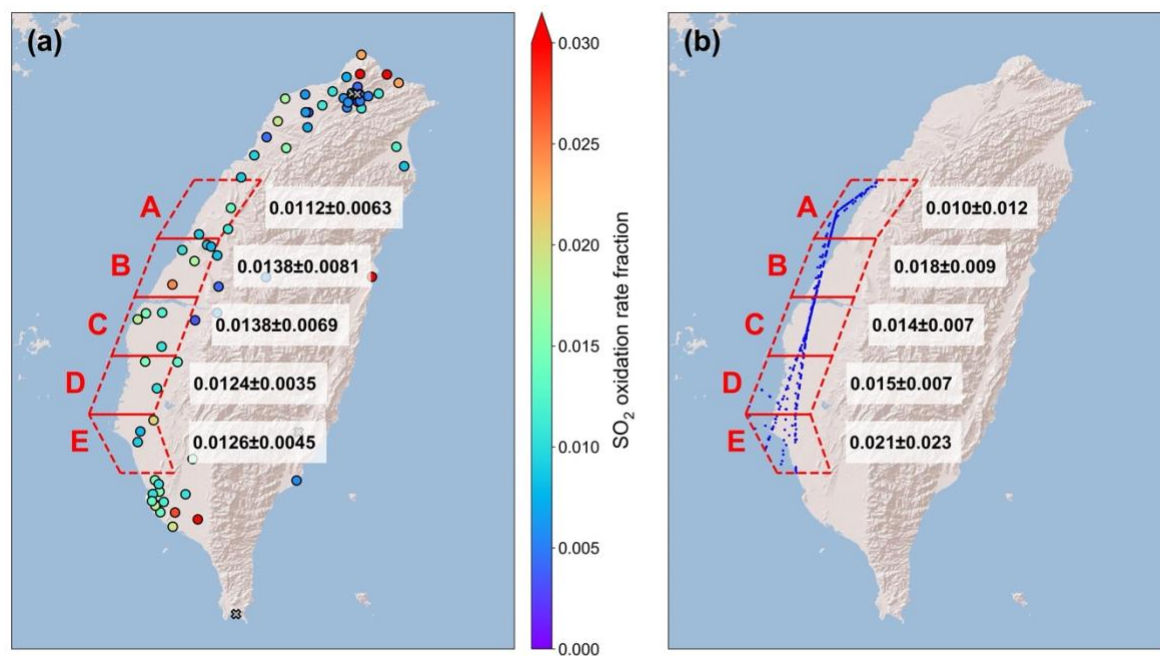
Figure 6: The average SO_2 oxidation fractions of the rate of loss of OH for the selected regions at the surface (a) and in the air (b). Scatter points in (a) show the SO_2 oxidation fraction of the rate of loss of OH at each EPA station. The flight tracks at 600 m are
505 **indicated as blue scattered lines in (b). The maps were generated using the Matplotlib Basemap Toolkit version 1.2.0 (https://matplotlib.org/basemap/index.html).**